Eur. Phys. J. B **52**, 521–529 (2006)
DOI: 10.1140/epjb/e2006-00333-4

THE EUROPEAN PHYSICAL JOURNAL B

The spin-2 antiferromagnet on the Bethe lattice

A. Erdinç, O. Canko, and E. Albayrak[a]

Erciyes University, Department of Physics, 38039, Kayseri, Turkey

Received 10 February 2006 / Received in final form 18 April 2006
Published online 21 August 2006 –

Abstract. The complete phase diagrams of the antiferromagnetic spin-2 Blume-Capel Ising system is studied on the Bethe lattice by the use of exact recursion relations. In order to specify the states of the system, i.e. the different spin configurations, the ground state phase diagram is obtained on the $(H/|J|, D/|J|)$ plane corresponding to the reduced external magnetic and crystal fields, respectively. As a result, the thermal change of the order-parameters, the magnetisations belonging to the two sublattice system, was investigated to obtain the full phase diagrams of the system on the $(H/|J|, kT/|J|)$ planes. The behavior of the order-parameters with respect to the external magnetic field was also studied for the given values of $D/|J|$. Besides the interesting thermal and external magnetic field change of the sublattice magnetisations, the system also exhibits interesting critical behaviors including first- and second-order phase transitions, therefore, triciritical points and the reentrant behavior. The calculations are carried out for the coordination number $q = 4$, corresponding to the square lattice, only.

PACS. 05.50.+q Lattice theory and statistics (Ising, Potts, etc.) – 05.70.Fh Phase transitions: general studies – 64.60.Cn Order-disorder transformations; statistical mechanics of model systems – 75.10.Hk Classical spin models

1 Introduction

According to the Hund's rule the spins of Fe^{II} ions are spin-2 and it is experimentally found that these ions have anisotropy [1]. The spin systems are called antiferromagnetic or ferromagnetic depending on the sign of the bilinear interaction J of the nearest-neighbor spins, that is the antiferromagnetism corresponds to $J < 0$ in which case the lattice must be divided into two sublattices while the latter case corresponds $J > 0$. Therefore, we were encouraged to study the spin-2 antiferromagnetic Ising model with a crystal field.

The Ising models including the crystal field or the single ion anisotropy was firstly introduced as a spin-1 Ising model and studied within the mean-field approximation by Capel and independently by Blume in 1966 [2], therefore, it is called as a Blume-Capel model. Since then the spin-1 system has been studied with many techniques and it was found that it exhibits very interesting and rich critical phenomenons. The next integer-spin model is the spin-2 Ising model which has the spin values $\pm 2, \pm 1$ and 0, i.e. the latter three values are also the spin values for the spin-1, therefore the critical behaviors of the spin-2 system must also be very interesting to study, but somehow the system has not received well deserved attention so far. The reason for this, since the exact solutions are generally unavailable, therefore, they must be accompanied with numerical analysis and for such a high spin value it is really very hard to find and distinguish all the solutions of the model.

Therefore, the spin-2 Ising ferromagnet, $J > 0$, has been studied with some different techniques and models such as; the general expressions for evaluating the second-order phase transition line and tricritical point of the Ising model with and without the crystal and transverse magnetic fields (TIM) [3], the effect of the transverse crystal field and transverse external magnetic field on the phase diagrams, magnetization, quadrupolar moments, internal energy and specific heat of the system [4] and [5], respectively, the properties of the ground state TIM with the presence of a crystal field on honeycomb lattice ($q = 3$) [6], the random-field Ising model (RFIM) in the presence of the crystal field on honeycomb, square and the simple cubic lattices with the random field is on and off [7] are all studied within the effective field theory with correlations. The magnetization and ground state structures of Ising integer-spin system including spin-2 with bilinear and biquadratic exchange interactions were investigated by making use of the four-spin model approximation [8]. The quenched diluted ferromagnet has been studied theorethically with a probability distribution method based on the use of the Tucker's generalized Van der Waerden identities [9] and with site dilution in a transverse field was treated by using an effective field method within the framework of a single site cluster theory [10], where the results without dilution are also presented. The bimodal and

[a] e-mail: albayrak@erciyes.edu.tr

trimodal random-field spin-2 Ising systems in a transverse field were investigated by combining the pair approximation with the discretized path integral representation [11], respectively, and the matrix product approach was used to construct all optimum ground states of general anisotropic spin-2 chains with nearest-neighbor interactions and common symmetries [12]. We should also note that the spin-S system for $(S > 1)$, where also the spin-2 calculations and results were given as a part of the work, has been studied, see references in [11].

For the antiferromagnetic case, $J < 0$, as far as we know there are not any studies for the classical Ising model. In spite of this, the other model which is used to study the magnetic spin systems is the quantum mechanical Heisenberg model, therefore, at least we can mention few works for the spin-2 quantum antiferromagnets such as; an efficient projector Monte Carlo method was used to calculate the numerical solution of the spin-2 Heisenberg antiferromagnetic chains [13], the optimum ground state approach was used to construct exact nontrivial ground states of spin-2 quantum antiferromagnets on the hexagonal lattices [14] and the vertex state model approach was used to construct optimum ground states for a large class of quantum spin-2 antiferromagnets on the square lattice [15]. At this point, it should be mentioned that the antiferromagnetic case has only been studied at the ground state level but as mentioned above the spin-2 system does deserve to be studied for higher temperatures as well.

We should also mention that the exact solutions for the realistic systems on regular lattices are generally unavailable, therefore, one usually relies on approximation methods to obtain, at least, a qualitative picture for the phase diagrams of the considered system at hand. One may even introduce a lattice-like fictitious tree to find exact or approximate solutions of the model. A Bethe lattice is such a lattice, which is an infinitely Cayley or regular tree i.e. a connected graph without circuits and historically gets its name from the fact that its partition function is exactly that of an Ising model in the Bethe approximation [16]. The importance is that the Bethe lattice is an infinite tree gives us the negligible boundary effects, therefore, far from the boundary sites that is deep inside the Cayley tree, now Bethe lattice, all the sites become equivalent, thus studying the behavior of one spin, named as the central spin, is enough to obtain the full picture of the system. We should also comment that the Bethe lattice calculations provides exact solutions and results of which qualitatively better approximations for the regular lattices than solutions obtained by the conventional mean-field theories [17]. In addition, the cluster variation method in the pair approximation studies on regular lattices yield results that are exact for the same model on the Bethe lattice [18]. Of course, the Bethe lattice considerations also have some limitations that is it predicts a transition temperature higher than that for a regular lattice and it is not reliable for predicting critical exponents [19], where also the correspondence of the Bethe lattice with regular lattices and real physical systems and whether it can be embedded into a finite-dimensional Euclidean space are also discussed. Therefore, in this work we have employed the use of the Bethe lattice in terms of the recursion relations [20] to study the spin-2 antiferromagnet.

The remaining part of the paper for the spin-2 antiferromagnetic Ising system is constructed as follows. In Section 2, besides the ground state phase diagram given on the $(H/|J|, D/|J|)$ plane, the exact formulation of the model is also presented. Section 3 is devoted to the thermal and external magnetic field variations of the sublattice magnetisations and to the phase diagrams of the system on the the $(H/|J|, kT/|J|)$ planes. In the final section, we present a brief summary, comparisons and some remarks.

2 The formulation in terms of the exact recursion relations

The Hamiltonian of the spin-2 antiferromagnetic $(J < 0)$ Blume-Capel (BC) model is given as

$$\mathcal{H} = -J \sum_{\langle ij \rangle} \sigma_i \sigma_j - D \sum_i \sigma_i^2 - H \sum_i \sigma_i, \qquad (1)$$

where each σ_i located at site i is a spin-2 with five discrete spin values, i.e. $\pm 2, \pm 1$ and 0, D and H denote the crystal and the external magnetic fields, respectively, and while the first sum runs over all the nearest-neighbor pairs, the last two sums run over all the sites.

Before obtaining the phase diagrams of the system on the $(H/|J|, kT/|J|)$ planes, first we have to study analytically the ground state phase diagram, the phase diagram of the system at zero absolute temperature, to determine the different configurations, i.e. ground states, of the system. The ground-state energy in units of $|J|$ and with crystal and external magnetic fields may be described by the following Hamiltonian:

$$\frac{E}{q|J|} = -\left[\frac{J}{|J|}\sigma_i\sigma_j + \frac{D}{q|J|}(\sigma_i^2 + \sigma_j^2) + \frac{H}{q|J|}(\sigma_i + \sigma_j)\right], \qquad (2)$$

where the bilinear interaction is restricted to the q nearest-neighbor pair of spins and $q = 4$ is taken. Then the ground state configurations corresponding to the spin values $\pm 2, \pm 1$ and 0 are obtained by comparing the values of the energy E as given in the above equation for different spin configurations and then the ground state of the system is the one with the lowest energy for given values of the system parameters. As a result, the obtained ground state configurations, labeled with the values (σ_A, σ_B) for the sublattices, are presented in Figure 1. The coordinates $(H/|J|, D/|J|)$ of the multiple phase points are indicated with the solid circles and given as

$A_1 \to (-8, 0)$, $A_2 \to (-10, -2)$,
$A_3 \to (-6, -2)$, $A_4 \to (-2, -2)$ for $H/|J| < 0$
and
$B_1 \to (8, 0)$, $B_2 \to (2, -2)$,
$B_3 \to (6, -2)$, $B_4 \to (10, -2)$ for $H/|J| > 0$.

In addition to these, the solid lines separating the different ground state configurations may be named as the multiphase lines, since the corresponding separated configurations coexist on these lines. As a result, the multiphase points A_1 and B_1 are isolated on the $D/|J| = 0$ line and the others $A_2 \rightarrow A_4$ for $H/|J| < 0$ and $B_2 \rightarrow B_4$ for $H/|J| > 0$ are actually connected with a multiphase line starting from A_2 and ending on the B_4 as seen on the ground state phase diagram corresponding to the value of $D/|J| = -2.0$. It is interesting to note that even if the multiphase line starting with A_4 and ending on B_2 separates the $(-2, 2)$ configuration from the $(0, 0)$ one, the configuration $(-1, 1)$ also appears on this line which is contrary to the other multiphase lines of the diagram. Therefore, in order for the ground state phase diagram to shed light in obtaining the full phase diagrams of the model, we have divided it into three regions by the $D/|J| = 0$ line, passing through the isolated multiphase points A_1 and B_1, and $D/|J| = -2.0$ line, passing through the multiphase points $A_2 \rightarrow A_4$ and $B_2 \rightarrow B_4$ which are actually on the multiphase lines starting with A_2 and ending on point B_4, corresponding to the range of values of $D/|J|$ in the intervals of $(\infty, 0)$, $(0, -2)$ and $(-2, -\infty)$. Thus, the dashed lines separate three regions in the ground state phase diagram, indicated with roman numbers I, II and III, showing some characteristic differences depending on the number of different configurations of the system labeled with (σ_A, σ_B) pairs. Consequently, in order to study the thermal and external magnetic field change of the order-parameters to obtain the phase diagrams at higher temperatures we have chosen the values of crystal fields from these three regions besides the crystal field values for the lines passing the multiphase points, which are enough to obtain the complete phase diagrams of the model. For the final word, we should also note that the ground state phase diagram is symmetric with respect to $H/|J| = 0$ line, i.e. invariant under the transformation $H \rightarrow -H$ and $\sigma \rightarrow -\sigma$.

In order to calculate the phase diagram of the system, first we have to obtain the formulation of the system on the Bethe lattice in terms of the recursion relations. Thus, let us start with the calculation of the partition function

$$Z = \sum_{\{\sigma\}} \exp(-\beta\mathcal{H}) = \sum_{Spc} P(Spc) = \sum_{\{\sigma\}} \exp[\beta(J \sum_{\langle ij \rangle} \sigma_i\sigma_j + D\sum_i \sigma_i^2 + H\sum_i \sigma_i)], \quad (3)$$

where $P(Spc)$ is considered as an unnormalized probability distribution over the spin configurations, $Spc \equiv \{\sigma_i, \sigma_j\}$, etc. If the Bethe lattice is cut in some central point deep inside with a spin σ_0, then it splits up into q identical branches whose number depends on the number of nearest-neighbors or the coordination numbers. Each of these branches is a rooted tree at the central-spin σ_0. This implies that $P(Spc)$, $Spc = \{\sigma_0\}$, is the spin-configuration with the spin value σ_0 at the central site and is given as

$$P(\sigma) = \exp\left[\beta(D\sigma_0^2 + H\sigma_0)\right] \prod_{k=1}^{q} Q_n\left(\sigma_0|\sigma^{(k)}\right), \quad (4)$$

where the suffix n expresses the fact that the sub-tree has n-shells, i.e. the number of steps from the root to the boundary sites. In equation (4) the function Q_n in the product is given as

$$Q_n(\sigma_0|\sigma^{(k)}) = \exp\left[\beta(J\sigma_0\sigma_1 + J\sum_{\langle ij \rangle} \sigma_i\sigma_j + D\sum_i \sigma_i^2 + H\sum_i \sigma_i)\right]. \quad (5)$$

The first summation in equation (5) is over all edges of the sub-tree other than the edge $(0, 1)$ and the summation over i is over all sites other than the central site σ_0. Now if the sub-tree, e.g. the upper sub-tree, is cut at the site 1 next to 0, then it also decomposes into q pieces: one being "trunk" $(0, 1)$ and the rest are the identical branches. Each of these branches is a sub-tree like the original, but with $n - 1$ shells and $q - 1$ neighbors. Therefore,

$$Q_n(\sigma_0|\{\sigma_1^k\}) = \exp[\beta(J\sigma_0\sigma_1 + D\sigma_1^2 + H\sigma_1)] \times \prod_{l=1}^{q-1} Q_{n-1}(\sigma_1^k|\{\tau_2^{(l)}\}), \quad (6)$$

where $\{\tau_2^{(l)}\}$ denotes the spin-configurations (other than $\sigma_1^{(k)}$) on the lth branch of the subtree. In order to obtain a formulation for the central spin σ_0 to be in a certain spin value with a certain probability as a result of its interaction with the external parameters and with its q nearest-neighbors of σ_1, we define

$$g_n(\sigma_0) = \sum_{\{\sigma_1\}} Q_n(\sigma_0|\{\sigma_1\}), \quad (7)$$

where the summation is taken over σ_1, since the central spin interacts only with its q nearest neighbors. Thus, from equations (6) and (7) we obtain

$$g_n(\sigma_0) = \sum_{\{\sigma_1\}} \exp[\beta(J\sigma_0\sigma_1 + D\sigma_1^2 + H\sigma_1)] \times [g_{n-1}(\sigma_1)]^{q-1}, \quad (8)$$

which varies depending on the spin values, i.e. for spin-2 they are $\pm 2, \pm 1$ and 0, and the system parameters. For each discrete spin values of σ_0, the nearest-neighbor spin can take five discrete values, $\pm 2, \pm 1$ and 0, therefore we obtain five different g_n functions for each value of σ_0. Therefore, for $\sigma_0 \equiv \pm 2$ we get

$$\begin{aligned} g_n(\pm 2) &= \sum_{\sigma_1} \exp[\beta(\pm 2J\sigma_1 + D\sigma_1^2 + H\sigma_1)] \times [g_{n-1}(\sigma_1)]^{q-1} \\ &= \exp[\beta(\pm 4J + 4D + 2H)][g_{n-1}(+2)]^{q-1} \\ &\quad + \exp[\beta(\mp 4J + 4D - 2H)][g_{n-1}(-2)]^{q-1} \\ &\quad + \exp[\beta(\pm 2J + D + H)][g_{n-1}(+1)]^{q-1} \\ &\quad + \exp[\beta(\mp 2J + D - H)][g_{n-1}(-1)]^{q-1} \\ &\quad + [g_{n-1}(0)]^{q-1}, \end{aligned} \quad (9)$$

when $\sigma_0 \equiv \pm 1$ we obtain

$$\begin{aligned} g_n(\pm 1) &= \sum_{\sigma_1} \exp[\beta(\pm J\sigma_1 + D\sigma_1^2 + H\sigma_1)] \times [g_{n-1}(\sigma_1)]^{q-1} \\ &= \exp[\beta(\pm 2J + 4D + 2H)][g_{n-1}(+2)]^{q-1} \\ &\quad + \exp[\beta(\mp 2J + 4D - 2H)][g_{n-1}(-2)]^{q-1} \\ &\quad + \exp[\beta(\pm J + D + H)][g_{n-1}(+1)]^{q-1} \\ &\quad + \exp[\beta(\mp J + D - H)][g_{n-1}(-1)]^{q-1} \\ &\quad + [g_{n-1}(0)]^{q-1}, \end{aligned} \tag{10}$$

and for the last spin value, i.e. $\sigma_0 \equiv 0$, we calculate as

$$\begin{aligned} g_n(0) &= \sum_{\sigma_1} \exp[\beta(D\sigma_1^2 + H\sigma_1)] \times [g_{n-1}(\sigma_1)]^{q-1} \\ &= \exp[\beta(4D + 2H)][g_{n-1}(+2)]^{q-1} \\ &\quad + \exp[\beta(4D - 2H)][g_{n-1}(-2)]^{q-1} \\ &\quad + \exp[\beta(D + H)][g_{n-1}(+1)]^{q-1} \\ &\quad + \exp[\beta(D - H)][g_{n-1}(-1)]^{q-1} \\ &\quad + [g_{n-1}(0)]^{q-1}. \end{aligned} \tag{11}$$

Finally, the four recursion relations are obtained in terms of the five g_n functions corresponding to each of the spin values $\pm 2, \pm 1$ and 0, therefore, dividing these g_n functions with one of the g_n function, let's say with $g_n(0)$, we obtain the recursion relations as

$$\begin{aligned} X_n &= \frac{g_n(+2)}{g_n(0)}, \quad Y_n = \frac{g_n(-2)}{g_n(0)}, \\ Z_n &= \frac{g_n(+1)}{g_n(0)}, \quad \text{and} \quad W_n = \frac{g_n(-1)}{g_n(0)}, \end{aligned} \tag{12}$$

which may be calculated explicitly by inserting the g_n functions given in equations (9–11) into the last equation.

In order to obtain the order-parameters in terms of these four recursion relations, first the partition function

$$Z = \sum_{\{\sigma_0\}} \exp\left[\beta\left(D\sigma_0^2 + H\sigma_0\right)\right] [g_n(\sigma_0)]^q, \tag{13}$$

should be obtained in terms of g_n functions as

$$\begin{aligned} Z &= e^{\beta(4D+2H)}[g_n(+2)]^q + e^{\beta(4D-2H)}[g_n(-2)]^q \\ &\quad + e^{\beta(D+H)}[g_n(+1)]^q + e^{\beta(D-H)}[g_n(-1)]^q + [g_n(0)]^q. \end{aligned} \tag{14}$$

Thus using the usual definition of the dipolar order-parameter, the magnetization,

$$M = Z^{-1} \sum_{\{\sigma_0\}} \sigma_0 \; P(\sigma_0), \tag{15}$$

which may be calculated explicitly in terms of the recursion relations by inserting the partition function and then doing the necessary calculations over the spin values as

$$\begin{aligned} M &= Z^{-1} \sum_{\{\sigma_0\}} \sigma_0 e^{\beta(D\sigma_0^2 + H\sigma_0)} [g_n(\sigma_0)]^q \\ &= \frac{2e^{4\beta D}[e^{2\beta H} X_n^q - e^{-2\beta H} Y_n^q] + e^{\beta D}[e^{\beta H} Z_n^q - e^{-\beta H} W_n^q]}{e^{4\beta D}[e^{2\beta H} X_n^q + e^{-2\beta H} Y_n^q] + e^{\beta D}[e^{\beta H} Z_n^q + e^{-\beta H} W_n^q] + 1}. \end{aligned} \tag{16}$$

The recursion relation equations, i.e. equation (12), form an iteration sequence $\{X_n, Y_n, Z_n, W_n\}$, which in the thermodynamic limit converges to stable fixed points. By the use of the expression for the magnetization these points completely define the possible states of the system. Using equations (9–12) and (14), we can also write the expression for the free energy, which is used to obtain the first-order phase transition temperatures, as

$$\begin{aligned} -\beta F = \frac{\ln Z}{N} &= \ln[e^{\beta(4D+2H)} X_n^q + e^{\beta(4D-2H)} Y_n^q \\ &\quad + e^{(D+H)} Z_n^q + e^{\beta(D-H)} W_n^q + 1] \\ &\quad + \frac{q}{2-q} \ln[e^{\beta(4D+2H)} X_n^{q-1} \\ &\quad + e^{\beta(4D-2H)} Y_n^{q-1} \\ &\quad + e^{(D+H)} Z_n^{q-1} + e^{\beta(D-H)} W_n^{q-1} + 1], \end{aligned} \tag{17}$$

where we have used the fact that deep inside the Bethe lattice, that is in the thermodynamic limit as $n \to \infty$, all the sites are equivalent.

In the antiferromagnetic coupling, in order to simulate the system we have to introduce two-sublattices, i.e. A and B. Hence the order-parameters belonging to each sublattice, the sublattice magnetisations, since each spin only interacts with its nearest neighbors, could be written as

$$\{M\} \to \begin{matrix} \{M_A\} & \text{for even n} \\ \{M_B\} & \text{for odd n} \end{matrix} \tag{18}$$

or equivalently these could be written in terms of the recursion relations as

$$\{X_n, Y_n, Z_n, W_n\} \to \begin{matrix} \{X_n^A, Y_n^A, Z_n^A, W_n^A\} & \text{for even n} \\ \{X_n^B, Y_n^B, Z_n^B, W_n^B\} & \text{for odd n.} \end{matrix} \tag{19}$$

The remarkable points of this approach are that non-staggered phases are described by the single fixed points $\{X_n, Y_n, Z_n, W_n\} \to \{X, Y, Z, W\}$, while the staggered phases appear as two-cycle double points [21] as indicated above.

Now, we are ready to investigate the thermal and external magnetic field variations of the sublattice magnetisations for given values of the crystal field, which were chosen from each of these three regions and for $D/|J| = 0$ and $D/|J| = -2.0$, i.e. multiphase point lines, as indicated in the ground state phase diagram, to obtain the phase diagrams of the system on the $(H/|J|, kT/|J|)$ plane for $q = 4$ only.

3 The complete phase diagrams and the behaviors of the sublattice magnetisations

In order to study the multicritical behaviors of the antiferromagnetic spin-2 BC model in an external magnetic field on the Bethe lattice, one has to study the thermal variations of the order-parameters and the free energy of the system. Therefore, the second-order phase transition

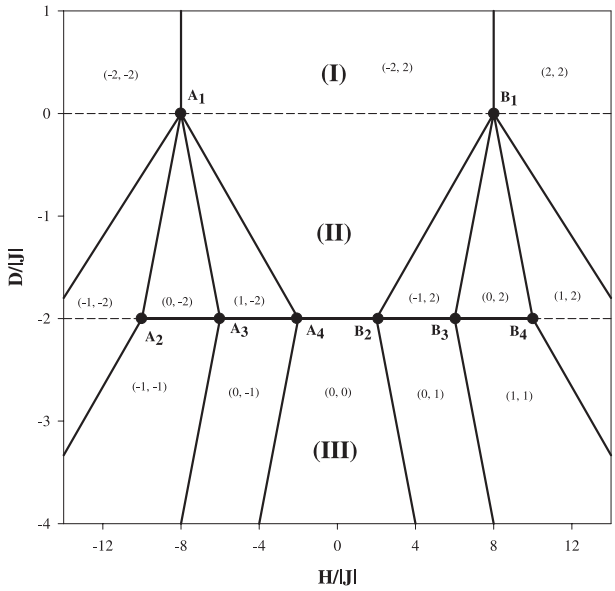

Fig. 1. The ground state phase diagram for the spin-2 antiferromagnet. See text for the details.

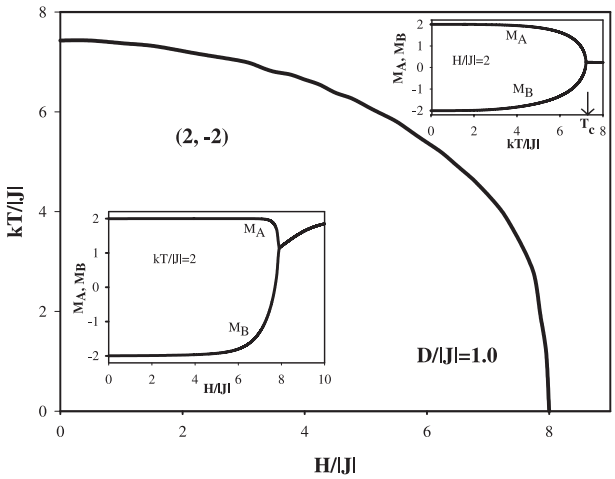

Fig. 2. The phase diagram on the $(H/|J|, kT/|J|)$ plane for $D/|J| = 1.0$ chosen from Region I of Figure 1. The system only gives second-order phase transitions as seen in the inset figures for thermal and magnetic field change of M_A and M_B. The second-order phase transition line separates the antiferromagnetic phase (2, −2) from the disordered phase and the ferromagnetic phase (2, 2) is only seen on the $kT/|J| = 0$ line with $H/|J| \geq 8$.

temperatures, T_c, are defined as the temperature at which the sublattice magnetisations become equal to each other, while at the first-order phase transition temperatures, T_t, the sublattice magnetisations show jump discontinuity or equivalently the temperature at which the free energy values corresponding to the different solutions of the model become equal. Thus, the phase diagrams of the model was constructed on the $(H/|J|, kT/|J|)$ planes for given values of $D/|J|$ by locating the places of these critical temperatures. In the phase diagrams the solid and dashed lines correspond to the second- and first-order phase transition temperatures and the different phase regions are indicated with the values of (σ_A, σ_B). We should also mention that by using the knowledge of the ground state phase diagram these regions corresponding to the different spin configurations are separated by the use of solid triangles. In order for this study to be more intelligible, whenever it is possible we have given the thermal and external magnetic field change of the sublattice magnetisations as the insets in the phase diagrams, otherwise they are separately displayed. In addition to these, we have also indicated the second- and first-order phase transition temperatures with T_c and T_t, respectively, together with an arrow for the thermal change of the sublattice magnetization figures. As it was mentioned above, the phase diagrams of the system are obtained for five values of the crystal fields corresponding to the regions I, II and III and, to the $D/|J| = 0$ and $D/|J| = -2.0$ lines passing through the multiphase points, where the part of the latter is actually a multiphase line starting from A_2 and ending at B_4, as shown in the ground state phase diagram (Fig. 1) of the model. As a result, we have studied the phase diagrams of the model for $H/|J| > 0$ because of symmetry with respect to $H/|J| = 0$ line for five different values of the crystal field as follows:

Region I: the phase diagram is obtained for $D/|J| = 1.0$ chosen from region I above the dashed line passing through $D/|J| = 0.0$ line. As shown in Figure 2, the antiferromagnetic region, i.e. (2, −2) phase, is separated from the disordered phase with the second-order phase transition line. The thermal and magnetic field variations of the sublattice magnetisations, M_A and M_B, are shown as inset figures obtained for $H/|J| = 2$ and $kT/|J| = 2$, respectively. As seen in the inset for the thermal change of the sublattice magnetisations, M_A and M_B start from 2 and −2 at zero temperature and as the temperature increases M_A decreases and M_B increases and they combine at T_c. We have also presented the magnetic field change of the magnetisations as an inset figure, where again M_A and M_B start from 2 and −2 at zero $H/|J|$ and as $H/|J|$ increases M_A decreases and M_B increases and they combine at some critical value of $H/|J|$. We should mention that the magnetization curves for the sublattices corresponding to the configuration (2, 2) as shown in the ground state phase diagram, i.e. at zero temperature, is totally ferromagnetic in nature. At nonzero temperatures with external magnetic fields acting on the system these magnetization curves never cut the $kT/|J| = 0$ line, therefore, no phase transitions are seen. As a result, the ferromagnetic phase with configuration (2, 2) can not be displayed in Figure 2, since the second-order phase transitions of the ferromagnetic case can only be obtained at zero $H/|J|$, i.e. the case of spontaneous magnetization.

The $D/|J| = 0$ line: in search of interesting multicritical behaviors, the phase diagram is calculated along the dashed line passing through the isolated multiphase points A_1 and B_1 and presented in Figure 3. The obtained phase diagram is similar with the previous one, i.e. Figure 2, but there are only two differences; the first one is the second-order line starts at a lower value of $kT/|J|$ at $H/|J| = 0$ and the other is that the appearance of the reentrant behavior. As seen in Figure 3, the second-order line start

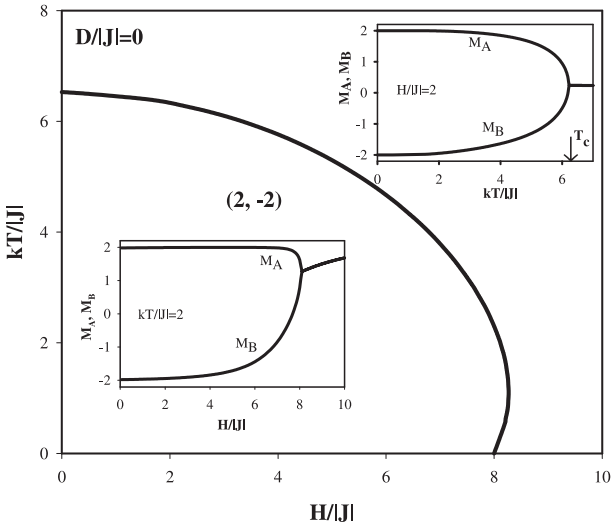

Fig. 3. Same as with Figure 2, but $D/|J| = 0$ chosen along the dashed line passing through the isolated multiphase points.

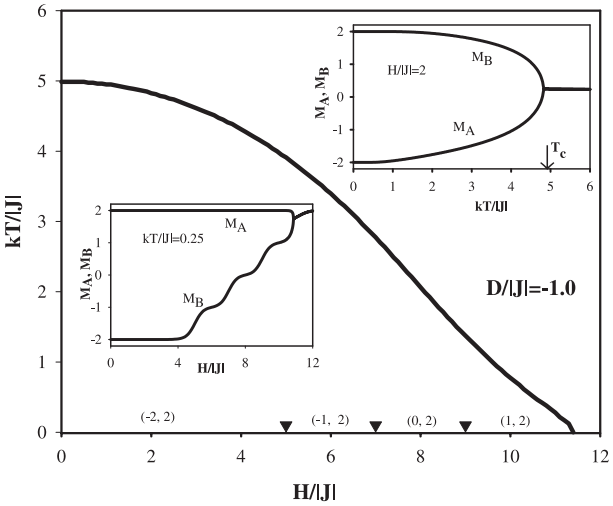

Fig. 4. Similar with Figure 2, but the phase diagram is obtained for region II of Figure 1 with $D/|J| = -1.0$. The second-order phase line is less sharp close to $kT/|J| = 0.0$ compared with the first two phase diagrams.

at zero temperature with $H/|J| = 8.0$ as expected from the ground state phase diagram and as the temperature increases this line extends beyond the $H/|J| = 8.0$ and as the temperature increases further the line passes the point $H/|J| = 8.0$ the second times in the opposite direction, thus presenting the reentrant behavior.

Region II: the phase diagram is obtained for $D/|J| = -1.0$ chosen from region II between the two dashed lines and exhibited in Figure 4. As seen in the ground state phase diagram, in moving on the positive $H/|J|$-axes starting from zero, one has to cross the multiphase lines, i.e. the first one of these separates the configuration $(-2, 2)$ from the configuration $(-1, 2)$, the second one separates the latter from the configuration $(0, 2)$, the next separates $(0, 2)$ from $(1, 2)$ and the final one separates $(1, 2)$ from $(2, 2)$ configuration. The ranges of these configurations, i.e. the beginning and ending $H/|J|$ values for each configuration according to the ground state phase diagram, are labeled with solid triangles in the phase diagram on the $(H/|J|, kT/|J|)$ plane. The system again presents only second-order phase transitions, but now the second-order phase transition line goes to zero temperature at higher $H/|J|$. In the insets of the figure, we have only presented the thermal and magnetic field change of the sublattice magnetisations for the configuration $(2, -2)$ at $H/|J| = 2.0$ and $kT/|J| = 0.25$, respectively. Even if the different configurations, as seen in the ground state phase diagram, available at zero temperature which are indicated with solid triangles in the phase diagram, i.e. Figure 4, but which are not easily distinguished at higher temperatures. The reason of this, even though as the temperature increases a little, these configurations disappear gradually, for example, in the inset figure for $kT/|J| = 0.25$ the magnetization curves present flatness for the corresponding configurations, but they disappear as the temperature increases further.

The $D/|J| = -2.0$ line: the drawn dashed line actually passes through the multiphase line starting from the multiphase point A_2 and ending on the multiphase point B_4 besides the other multiphase points, A_3, A_4, B_2 and B_3 at shown in the ground state phase diagram. Therefore, the obtained phase diagram is the most interesting and the complicated one of this work and is presented in Figure 5a. Starting from $H/|J| = 0$ and moving along the positive $H/|J|$-axes, one has to pass three multiphase points besides the multiphase line separating the different configurations of the model. The part of the multiphase line, i.e. $A_4 - B_2$, separates the configuration $(-2, 2)$ from $(0, 0)$, thus along this line both configurations exist besides the configuration $(-1, 1)$, which is only seen along this line for the ground state phase diagram. The system gives two first-order phase transitions for the configurations $(-2, 2)$ and $(-1, 1)$ at lower and higher $kT/|J|$ values, respectively, which is also indicated in Figures 5b(i) and 5b(ii) (obtained by lowering the temperature from above to see the initial values of the sublattice magnetisations, i.e. it is the same with the corresponding branch of the magnetisations given in (i)) for the thermal change of the sublattice magnetisations where at the critical value of $kT/|J|$ both of the magnetisations show jump discontinuity. The second part of the multiphase line $B_2 - B_3$ separates the configurations $(0, 1)$ and $(-1, 2)$, where for the first configuration only second-order and for the $(-1, 2)$ configuration only the first-order phase transitions are observed at higher and lower values of $kT/|J|$, respectively, thus for this range the model presents both first- and second-order phase transitions. The thermal change of the magnetisations for this case is illustrated in Figure 5b(iii) and 5b(iv), where the latter is again an extension of 5b(iii) as explained in the previous case, as seen the magnetisations start with the configuration $(-1, 2)$ at zero $kT/|J|$ and at the first T_t the magnetisations jump to the configuration $(0, 1)$ and eventually both of the magnetisations combine at the T_c. The last part of the multiphase line $B_3 - B_4$ separates the configurations $(0, 2)$ and $(1, 1)$.

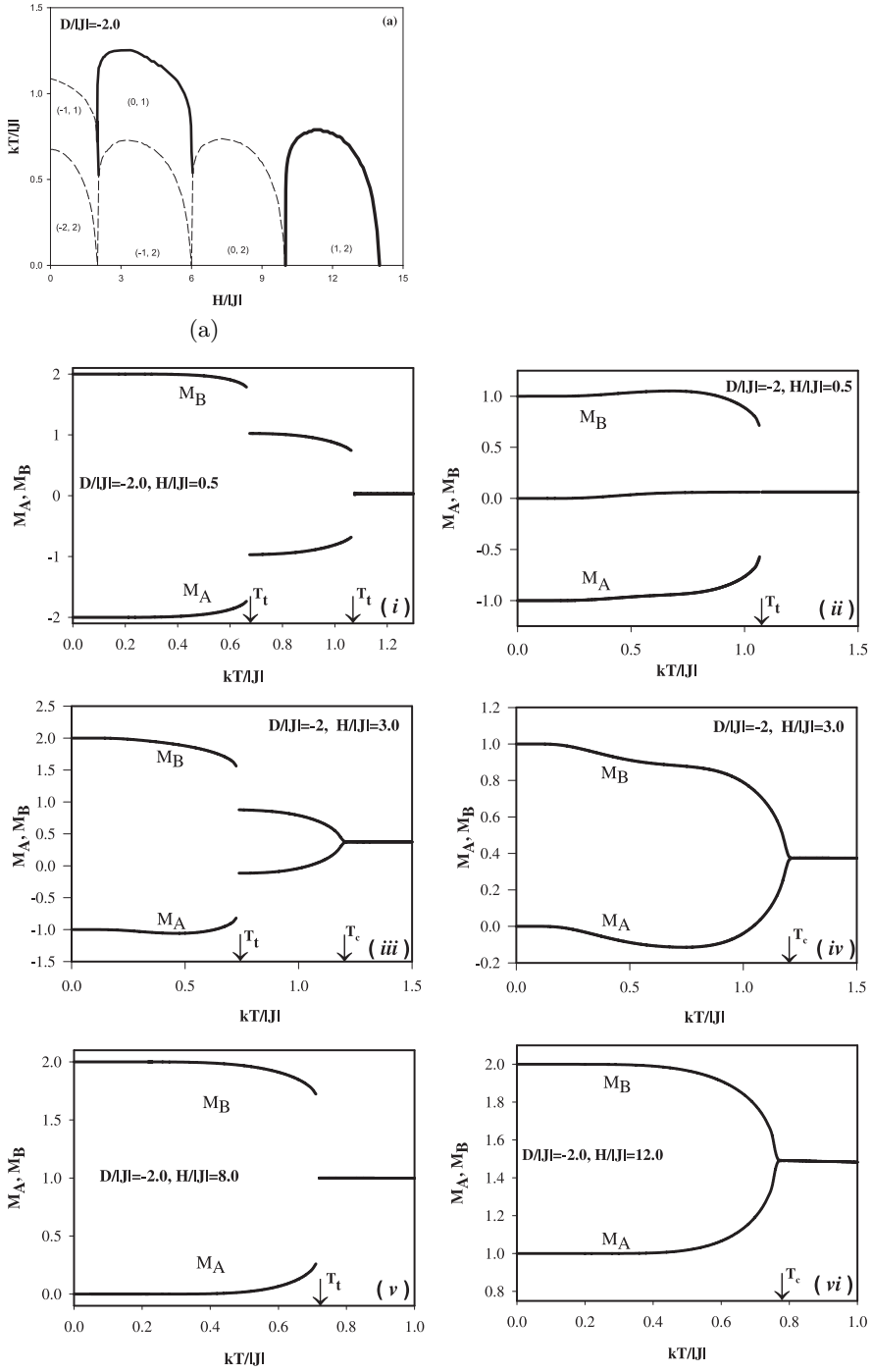

Fig. 5. (a) The phase diagram is obtained for $D/|J| = -2.0$, i.e. the second dashed line, containing the multiphase points and the multiphase line $A_4 - B_4$ of Figure 1 for positive $H/|J|$. The system shows both second- and first-order phase transitions, therefore tricritical points; (b) thermal variations of the sublattice magnetisations for the configurations indicated in the phase diagram; and (c) the splitting of the sublattice magnetisations corresponding to the magnetic field change obtained for $kT/|J| = 0.4$.

It should again be mentioned that in the phase diagram no solution was obtained for the totally ferromagnetic configuration (1, 1), since this ferromagnetic configuration gives phase transitions only at zero temperature. For nonzero temperatures because of the existence of the external magnetic field, this configuration is not seen in the phase diagram which is also explained previously for the configuration (2, 2) in Figure 2. As a result, the model shows only one first-order phase transition with the configuration (0, 2) for this part of the multiphase line and for which the thermal behaviors of M_A and M_B, given in Figure 5b(v), exhibits jump discontinuity. The multiphase line ends on the point B_4, therefore, the dashed line now only cuts the multiphase line separating the configurations (1, 2) and (2, 2), where again the configuration (2, 2) is totally ferromagnetic and no solution was found as in the configuration with (1, 1), thus this part of the phase diagram only presents second-order lines which is also seen in Figure 5b(vi) for the thermal variations of the sublattice magnetisations. We should also mention that the point where the second- and first-order phase lines connect are called as the tricritical point. Besides the phase diagram and the thermal variations of the sublattice magnetisations, we have also depicted the magnetic field change of the sublattice magnetisations along $kT/|J| = 0.4$ in the phase diagram. As the external magnetic field increases the sublattice magnetisations give five first-order and two second-order phase transitions indicated with arrows in Figure 5c in agreement with the corresponding phase diagram, i.e. Figure 5a.

Region III: the last phase diagram is obtained for $D/|J| = -4.0$, see Figure 6, which is below the second dashed line passing through the $D/|J| = -2.0$. Again in moving along the positive $H/|J|$-axis, one has to cross the configurations (0, 0), (0, 1), (1, 1), (1, 2) and (2, 2) as seen in the ground state phase diagram. In the phase diagram, we only find solutions belonging to the configurations (0, 1) and (1, 2) for which the sublattice magnetisations only show second-order phase transitions. In addition, the configurations (1, 1) and (2, 2) correspond to the ferromagnetic case and for negative bilinear interaction, i.e. antiferromagnetic case, again because of the external magnetic field these phases can not be seen which is also explained for Figures 2 and 5. The second-order lines, surround the phases with configurations (0, 1) and (1, 2), make similar closed peaks occurring at lower and higher external magnetic fields, respectively, separates these ordered phases from the disordered phase. In the inset figures for the thermal variations of M_A and M_B, the existence of the second-order phase transitions are clearly indicated. The magnetic field change of M_A and M_B is also given as an inset figure, where the two branches of the sublattice magnetisations make nice closed loops for the corresponding configurations in agreement with the phase diagram.

We should mention that the obtained rich phase diagrams are all in agreement with the thermal and magnetic field change of the sublattice magnetisations and with the ground state phase diagram.

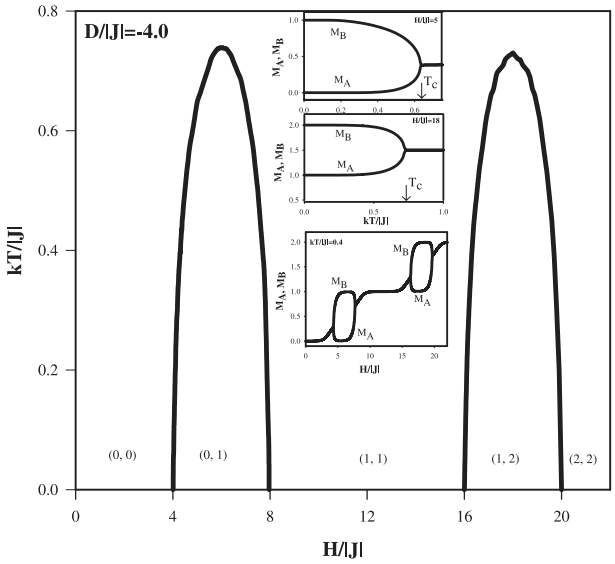

Fig. 6. The phase diagram is obtained for $D/|J| = -4.0$ chosen from Region III of Figure 1. The system shows only parabolic like second-order phase transition lines for the configurations (0, 1) and (1,2) which separates these ordered phases from the disordered phase. The phases (0, 0), (1, 1) and (2, 2) only exist at zero temperature. Thus, the thermal and magnetic field change of M_A and M_B are given in the inset figures for only (0, 1) and (1, 2) configurations.

4 Conclusion

The spin-2 Ising antiferromagnet was studied systematically; first in order to distinguish the different configurations of the Blume-Capel model we have obtained the ground state phase diagram on the $(H/|J|, D/|J|)$ plane. Then by choosing five different places in the ground state phase diagram, each having its own characteristic configurations, for five different values of the crystal field interactions the phase diagrams of the model were obtained on the $(H/|J|, kT/|J|)$ planes. We have also illustrated the thermal and external magnetic field variations of the order-parameters either as insets or separately. As a result, we have obtained some critical behaviors such as second- and first-order phase transitions, tricritical points and the reentrant behavior. Therefore, the obtained phase diagrams are very rich in content as we mentioned in the introduction.

In order to generalize the antiferromagnetic Blume-Capel spin-S system, i.e. $S = 1, 3/2, 2$, etc., we have to consider the typical phase diagrams of the model obtained for the values of $D/|J|$ as given in this work: when $D/|J| > 0$, the system is in the configuration corresponding to the maximum spin value $(S, -S)$ of spin-S system in which case the second-order phase transition lines separate the ordered phase from the disordered phase. As the values of $D/|J|$ becomes negative the transitions are seen to be second-order type but as we get closer and closer to the $D/|J| = -2$ the first-order transitions occur and the configurations can be classified from left to the right on the $H/|J|$-axes as $(-S + i, S)$ with $(i = 0, 1, ..., 2S - 1)$

for the spin-S system again. The corresponding configurations of the latter now can be exactly distinguished for $D/|J| = -2$, since the phase regions are now separated by the critical lines of the first- or the second-order type. In this case, each of the ground state configurations $(-S+i, S)$ make sequential closed loops on the top of each other as the temperature increases in which case the corresponding configurations can easily be obtained by increasing and decreasing the $(-S+i, S)$ configuration by one, respectively. Finally, for $D/|J| < -2$, the system only gives second-order phase transitions in the form of closed peaks, as the $H/|J|$ values increase the spin configurations for the integer spin-S system as starting from the lowest spin values, i.e. $(S_a = 0, S_b = 0)$, then these spin values increase one by one for S_a and S_b for which the loops are seen only for $S_a \neq S_b$ and for the half-integer system the phase diagram starts with a half-closed loop with the spin configuration $(S_a = 1/2, S_b = -1/2)$ again the spin values increase one by one for S_a and S_b with $S_a \neq S_b$ again, sequentially. What we are saying above can easily be understood when one compares Figures 2 and 3 of [22] for spin-1, Figure 1 of [23] for spin-3/2 and all the phase diagrams of this work for spin-2.

In conclusion, we have studied very thoroughly and in detail the spin-2 Ising antiferromagnet on the Bethe lattice and we have tried to generalize by using the obtained phase diagrams of spin-1 [22], spin-3/2 [23], spin-2 of this work and for higher spin-S values intuitively.

References

1. C. Mathoniere, C.J. Nutall, S.G. Carling, P. Day, Inorg. Chem. **35**, (1996) 1201
2. H.W. Capel, Physica **32**, 966 (1966); M. Blume, Phys. Rev. **141**, 517 (1966)
3. W. Jiang, G.-Z. Wei, Z.-H Xin, J. Magn. Magn. Mater. **220**, 96 (2000)
4. W. Jiang, G.-Z. Wei, Z.-H. Xin, Phys. Stat. Sol. (b) **221**, 759 (2000)
5. W. Jiang, G.-Z. Wei, Z.-H. Xin, Phys. Stat. Sol. (b) **225**, 215 (2001)
6. W. Jiang, G.-Z. Wei, D. An, Z. Qi, Chinese Phys. **11**, 823 (2002)
7. Y.Q. Liang, G.-Z. Wei, Q. Zhang, Chinese Phys. Lett. **21**, 378 (2004); Y.Q. Liang, G.-Z. Wei, Song L.-L., Song G.-L., Zang S.-L, Commun. Theo. Phys. **42**, 623 (2004)
8. T. Iwashita, R. Satou, T. Imada, T. Idogaki, Physica B **284**, 1203 (2000)
9. H. Elmir, M. Saber, J.W. Tucker, J. Magn. Magn. Mater. **138**, 76 (1994)
10. M. Saber, J.W. Tucker, Physica A **217**, 407 (1995)
11. O. Canko, E. Albayrak, M. Keskin, J. Magn. Magn. Mater. **294**, 63 (2005); O. Canko, E. Albayrak E, Phys. Lett. A **340**, 18 (2005)
12. M.A. Ahrens, A. Schadschneider, J. Zittartz, Europhys. Lett. **59**, 889 (2002)
13. G. Sun, Phys. Rev. B **51**, 8370 (1995)
14. M.A. Ahrens, A. Schadschneider, J. Zittartz, Phys. Rev. B **71**, 174432 (2005)
15. H. Niggemann, A. Klümper, J. Zittartz, Eur. Phys. J. B **13**, 15 (2000)
16. M. Kurota, R. Kikuchi, T. Watari, J. Chem Phys. **21**, 434 (1953); C. Domb, Adv. Phys. **9**, 208 (1960)
17. C.-K. Hu, N.Sh. Izmailian, Phys. Rev. E **58**, 1644 (1998); N.Sh. Izmailian, C.-K. Hu, Physica A **254**, 198 (1998)
18. J.W. Tucker, J. Magn. Magn. Mater. **195**, 733 (1999); E. Albayrak, M. Keskin, J. Magn. Magn. Mater. **261**, 196 (2003); E. Albayrak, A. Yigit, Physica A **349**, 471 (2005); E. Albayrak, A. Yigit, Phys. Stat. Sol. (b) **242**, 1510 (2005)
19. C.-K. Hu, N.Sh. Izmailian, K.B. Oganesyan, Phys. Rev. E **59**, 6489 (1999)
20. R.J. Baxter, *Exactly Solvable Models in Statistical Mechanics* (Academic Press, New York, 1982)
21. A.Z. Akheyan, N.S. Ananikian, J. Phys. A **29**, 721 (1996); N.S. Ananikian, A.R. Avakian, N.Sh. Izmailian, Physica A **172**, 391 (1991); A.Z. Akheyan, N.S. Ananikian, Phys. Lett. **186A**, 171 (1994); A.Z. Akheyan, N.S. Ananikian, JETP **107**, 196 (1995)
22. J.D. Kimel, P. Arne Rikvold, Y.-L. Wang, Phys. Rev. B **45**, 7237 (1992)
23. M. Keskin, M.A. Pınar, A. Erdinç, O. Canko, Phys. Lett. A **353**, 116 (2006)